JMR Abstracts

Acting Editor-in-Chief: Robert P. Frankenthal • Associate Editors: Shigeyuki Somiya, Heinrich J. Wollenberger

Volume 14, Number 5

Abstracts for May 1999 Journal of Materials Research

TABLE OF CONTENTS

RAPID COMMUNICATIONS

Critical undercoolings for the formation of metastable phase and its morphologies solidified from undercooled Fe–Co melts M. Li, G. Song, G. Yang, Y. Zhou

Effects of thermal annealing on the dielectric properties of Pb(Zn_{1/3}Nb_{2/3})O₃-based ceramics E. Xia, X. Yao

Lower air-crystallization temperature and nanostructured yttria-doped tetragonal zirconia polycrystal ceramics by seeding assisted chemical coprecipitation P. Durán, J. Tartaj, J.F. Fernández, C. Moure

Synthesis of large-size β -Si₃N₄ crystals K. Furuya, K. Matsuo, F. Munakata, Y. Akimune, J. Ye, Y. Yamamoto, I. Ishikawa

Subsolidus phase equilibria in the La_2O_3 -CeO₂-Co₂O₃ system M. Hrovat, J. Holc, S. Bernik

ARTICLES

Effect of $P_{\mbox{O2}}$ and Ag on the phase formation of the Bi(Pb)-2223 superconductor

W. Wong-Ng, L.P. Cook, W. Greenwood

Entrapment of elongated and crystallographically aligned pores in YBa₂Cu₃O_{7-y} melt-textured with BaCeO₃ addition C-J. Kim, G-W. Hong, S-J.L. Kang

Texture analysis and microstructural features in YBa₂Cu₃O_{6+x} zone-partial-melted samples with Y₂BaCuO₅ additions R. Cabré, E. Martínez, Jna. Gavaldà, R. Solé, J. Massons, C. Rillo, M. Aguiló, F. Díaz

Effects of inorganic components on the mechanical properties of inorganic-organic hybrids synthesized from metal alkoxides and polydimethylsiloxane

N. Yamada, I. Yoshinaga, S. Katayama

Promotion of phase transformation and single-phase formation in silver-doped Tl-Ba-Ca-Cu-O superconducting thin films H-S. Koo, T-Y. Tseng

A study of the dislocations in Si-doped GaAs comparing diluted Sirtl light-etching, electron-beam-induced current, and micro-Raman techniques

P. Martin, J. Jiménez, C. Frigeri, L.F. Sanz, J.L. Weyher

High-resolution x-ray diffraction study of $In_{0.25}Ga_{0.75}Sb/InAs$ superlattice

A. Vigliante, H. Homma, J.T. Zborowski, T.D. Golding, S.C. Moss

Temperature and porosity dependence of the thermoelectric properties of SiC/Ag sintered materials

K. Kato, K. Asai, Y. Okamoto, J. Morimoto, T. Miyakawa

Synthesis of Fe-rich Fe-Al nanocrystalline solid solutions using ball milling

H.G. Jiang, H.M. Hu, E.J. Lavernia

Solidification of undercooled molten Cu₃₀Ni₇₀ J.Z. Xiao, H.W. Kui

 $Characterization \ of \ Fe-Ni(C) \ nanocapsules \ synthesized \ by \ arc \ discharge \ in \ methane$

X.L. Dong, Z.D. Zhang, S.R. Jin, W.M. Sun, X.G. Zhao, Z.J. Li, Y.C. Chuang

Prediction of new additives for galvanizing process by the properties of their constituent chemical elements H.M. Jin, Y. Li, P. Wu

Piezoelectric and pyroelectric behavior of lead zirconate titanate-lead sulphide-glass nanocomposites T.K. Kundu, D. Chakravorty, L.E. Cross

A new method for the production of a molybdenum-zirconia cermet C.M. Lukaniuk, L.D. Schwartz, T.H. Etsell

Chemical synthesis and characterization of polyaniline-molybdenum trisulfide composite

F. Fusalba, D. Bélanger

The effects of nonhydrostatic compression and applied electric field on the electromechanical behavior of poled lead zirconate titanate 95/5-2Nb ceramic during the rhombohedral to antiferroelectric polymorphic transformation D.H. Zeuch, S.T. Montgomery, D.J. Holcomb

Synthesis of anorthite by the Pechini process and structural investigation of the hexagonal phase S-H. Hong, J.F. Young, P. Yu, R.J. Kirkpatrick

Calorimetric and high-resolution transmission electron microscopy study of nanocrystallization in zirconia gel J. Málek, T. Mitsuhashi, J. Ramírez-Castellanos, Y. Matsui

Morphological evolution of barium titanate synthesized in water in the presence of polymeric species R.B. Bagwell, J. Sindel, W. Sigmund

Characterization of sol-gel Pb(Zr_{0.53}Ti_{0.47})O_3 in the thickness range 0.25–10 μm

R. Kurchania, S.J. Milne

Properties of BaBi₂Ta₂O₉ thin films prepared by chemical solution deposition technique for dynamic random-access memory applications

C.R. Foschini, P.C. Joshi, J.A. Varela, S.B. Desu

Structure and growth of yttrium iron garnet thin films with enhanced magnetic properties by metalorganic chemical vapor deposition

V.N. Moorthy, S. Dhara, A.C. Rastogi, B.K. Das, D.V.S. Jain

JMR Abstracts provides a preliminary listing of titles and abstracts tentatively scheduled to appear in Journal of Materials Research at the time MRS Bulletin is published. Late schedule changes before JMR Is printed may result in articles being added or deleted. The Materials Research Society regrets any inconvenience that may result from schedule changes. Copyright 1999 by Materials Research Society. All rights reserved. ISSN: 1066-2375.

Planar defects in ZnO thin films deposited on optical fibers and flat substrates

L. Sagalowicz, G.R. Fox

Si₃N₄-SiC-Y₂O₃ ceramics derived from yttrium-modified block copolymer of perhydropolysilazane and hydroxy-polycarbosilane Y. Iwamoto, K. Kikuta, S. Hirano

Residual stress fields in sol-gel derived thin TiO₂ layers D.H.J. Teeuw, M. de Haas, J.Th.M. De Hosson

Microstructural evolution and mechanical properties of gas-pressure-sintered Si_3N_4 with Yb_2O_3 as a sintering aid K-M. Lee, W-H. Lee, Y-H. Koh, J-J. Choi, H-E. Kim, S.S. Baek

Experimental assessment of the inhibition of reduction of Ca²⁺-doped barium titanate in a reducing atmosphere T-T. Fang, J-T. Shuei

The effect of Zn(OH)₂ addition on the electrode properties of nickel hydroxide electrodes

J. Chen, D.H. Bradhurst, S.X. Dou, H.K. Liu

Synthesis and luminescence of the nanosized Ce-doped silica particles dispersed within the pores of mesoporous silica host W. Cai, Y. Zhang, L. Zhang

A self-propagating high-temperature synthesis method for synthesis of AlN powder

S-L. Chung, W-L. Yu, C-N. Lin

Synthesis of amorphous boron nitride from the molecular precursor ammonia-monochloroborane D.R. Ketchum, A.L. DeGraffenreid, P.M. Niedenzu, S.G. Shore

Fabrication of undoped near-monophase $Ba_2 Ti_9 O_{20}$ via rapid thermal processing

W. Lin, R.F. Speyer

Microstructure and thermokinetics analysis of CS AIN K. Chen, C. Ge, J. Li, W. Cao

Modeling studies of the effect of thermal and electrical conductivities and relative density on field-activated self-propagating combustion synthesis

E.M. Carrillo-Heian, O.A. Graeve, A. Feng, J.A. Faghih, Z.A. Munir Silicon nitride:

Enthalpy of formation of the α - and β -polymorphs and the effect of C and O impurties J. Liang, L. Topor, A. Navrotsky, M. Mitomo

Structural characterization of deuterated titanium thin films R. Checchetto, P. Scardi

Face-centered-cubic titanium: An artifact in titanium/aluminum multilayers J. Bonevich, D. van Heerden, D. Josell

Programmed substrate temperature ramping to increase nucleation density and decrease surface roughness during metalorganic chemical vapor deposition of aluminum R. Jonnalagadda, D. Yang, B.R. Rogers, J.T. Hillman, R.F. Foster, T.S. Cale

Corrosion performance of ferrous and refractory metals in molten salts under reducing conditions J.E. Indacochea, J.L. Smith K.R. Litko, E.J. Karell

Elastic modulus measurement of multilayer metallic thin films K-H, Cho, Y. Kim

Iron oxide films of a spinel structure from thermal decomposition of metal ion citrate complex N. Uekawa, K. Kaneko

Microcharacterization of liquid delivery metalorganic chemical vapor deposition processed thin film materials exhibiting giant magnetoresistance

M.L. Weaver, L.P.M. Brandao, H. Garmestani, E.S. Gillman, K.H. Dahmen, A. Morrone

Microstructural evolution of dense and porous pyroelectric Pb_{1-x}Ca_xTiO₃ thin films A. Seifert, L. Sagalowicz, P. Muralt, N. Setter

Micropyretic synthesis and leaching of MoSi₂ powders through an aluminothermic reaction

M. Fu. S. Penumella, J.A. Sekhar

Bombarding energy dependence of bonding structure in amorphous carbon interlayer and its effect on diamond nucleation U.C. Oh, D.G. Cheng, F.X. Lu, J.H. Je

The effect of growth condition on the structure of 2H–AlN films deposited on Si(111) by plasma-assisted molecular-beam epitaxy U. Kaiser, P.D. Brown, I. Khodos, C.J. Humphreys, H.P.D. Schenk, W. Richter

Low-temperature chemical vapor deposition of tantalum nitride from tantalum pentabromide for integrated circuitry copper metallization applications

X. Chen, G.G. Peterson, C. Goldberg, G. Neusca, H.L. Frisch, A.E. Kaloyeros, B. Arkles, J. Sullivan

The effects of capping barrier layers on the compositional and structural variations of integrated Pb(Zr,Ti)O₃ ferroelectric capacitor having the dimension $3 \times 3 \,\mu\text{m}^2$

C.S. Hwang, J.C. Shin, J.B. Lee, J. Park, Y.J. Cho, H.J. Kim, S.Y. Lee, S.O. Park

Formation of C54–TiSi₂ in titanium on nitrogen-implanted (001)Si with a thin interposing Mo layer S.L. Cheng, J.J. Jou, L.J. Chen, B.Y. Tsui

Niobium and zirconium tellurides thin films prepared by sputtering D. Pailharey, Y. Mathey, M. Kassem

Structure and optical properties of diamondlike carbon synthesized by plasma immersion ion processing X-M. He, K.C. Walter, D.Q. Li, M. Nastasi

Formation mechanism of spherical oxide particles containing dye S. Wu, C. Zhu

Preparation and enhanced photocatalytic oxidation activity of surface-modified CdS nanoparticles with high photostability M.Y. Han, W. Huang, C.H. Quek, L.M. Gan, C.H. Chew, G.Q. Xu, S.C. Ng

The phase separation mechanism of CaO– B_2O_3 – P_2O_5 in an electric field

W. Liu, X.M. Gu, K.M. Liang, H. Chen, Y.K. Zheng, S.R. Gu

Structure-property behavior during aging of sol-gel derived silica modified with Si–H and Si–CH₃ groups V.M. Sglavo, S. Diré, M. Ferrari

Bulk amorphous Pd–Ni–Fe–P alloys: Preparation and characterization T.D. Shen, Y. He, R.B. Schwarz

Pyrolysis of self-assembled organic monolayers on oxide substrates H. Shin, Y. Wang, U. Sampathkumaran, M.R. DeGuire, A.H. Heuer, C.M. Sukenik

Anodic dissolution of diamondlike carbon film-coated type 301 stainless steel

C. Srividya, I. Moskowitz, S.V. Babu

Influences of thermal annealing and humidity exposure on surface structure of (100) single-crystal MgO substrate M.P. Delplancke-Ogletree, M. Ye, R. Winand, J.F. de Marneffe, R. Deltour

88

Irreversible hydrogenation of solid C₆₀ with and without catalytic metals

E.L. Brosha, J. Davey, F.H. Garzon, S. Gottesfeld

Study on the structure of PbS nanoparticles coated with dialkyldithiophosphate S. Chen, W. Liu, L. Yu

Determination of elastic modulus of thin films and small specimens using beam bending methods J. Menčík, E. Quandt

RAPID COMMUNICATIONS

Critical undercoolings for the formation of metastable phase and its morphologies solidified from undercooled Fe-Co melts

M. Li, G. Song, G. Yang, Y. Zhou (Northwestern Polytechnical University)

The maximum undercoolings of 304, 318, 308, and 296 K were achieved respectively in Fe-22, 26, 30, and 34 at.% Co alloys. The metastable bcc phase nucleated from melts when undercoolings exceeded critical ones. The critical undercoolings for the formation of metastable bcc phase from Fe-22, 26, 30, and 34 at.% Co melts were 104, 156, 204, and 248 K, respectively. The morphologies of as-obtained metastable bcc phase exhibited five typical patterns: dendrite cores with primary and second arms, well-developed second arms, and radiated, lath, and platelike structures. Based on the classical nucleation theory, the solidification behavior of the melts was analyzed with regard to the metastable phase formation when the melts were undercooled greater than critical undercoolings. The formation of various morphologies was also evaluated to consider the solidification behavior of the undercooled melts. Order No.: JA905-001 © 1999 MRS

Effects of thermal annealing on the dielectric properties of Pb(Zn_{1/3}Nb_{2/3})O₃-based ceramics F. Xia, X. Yao

(Xi'an Jiaotong University)

Pb(Zn_{1/3}Nb_{2/3})O₃-based ceramics were thermally annealed at 700-900 °C for 4 h. Both the relative dielectric constant and dissipation factor in the vicinity of transition temperature were increased when the specimens were thermally annealed at 700-900 °C, but the diffusion factor was decreased. After thermal annealing, the maximum dielectric constant K_m was increased from about 11,000 to 26,000. These phenomena can be related to the domain wall motion and the elimination of internal stress. Order No.: JA905-002 © 1999 MRS

Lower air-crystallization temperature and nanostructured vttria-doped tetragonal zirconia polycrystal ceramics by seeding assisted chemical coprecipitation P. Durán, J. Tartaj, J.F. Fernández, C. Moure

(Instituto de Cerámica y Vidrio)

The crystallization temperature of yttria-doped tetragonal zirconia polycrystal (Y-TZP) amorphous precursors can be lowered 150 °C below that currently used (≥500 °C) if "seeding assisted chemical coprecipitation" is used. Completely crystallized Y-TZP nanocrystalline powder was obtained by calcining at 350 °C in air the Y-TZP precursors seeded with 10 wt% of nanometric (~8 nm) Y-TZP particles. The seed particles enhanced both the nucleation and the crystallization rates at lower temperatures. From such a powder, 99% dense and nanostructured (grain size <90 nm) Y-TZP bodies can be prepared by sintering below 1050 % Order No.: JA905-003 © 1999 MRS

Synthesis of large-size β -Si₃N₄ crystals K. Furuya, K. Matsuo, F. Munakata, Y. Akimune, J. Ye, Y. Yamamoto, 2 I. Ishikawa²

(¹Nissan Motor Company, Ltd., ²NISSAN ARC, Ltd.)

Large-sized β -Si₃N₄ crystals up to 10 mm in length and 0.3 mm in diameter with low impurity concentration are successfully grown from silicon melt in a nitrogen atmosphere. By controlling the concentration of impurities in the silicon melt, a new kind of β -Si₃N₄ crystal, that is, transparent coloring one with an absorption edge around wavelength of 520 nm, is obtained Order No.: JA905-004 © 1999 MRS

MRS BULLETIN/MARCH 1999

Electrodeposition of lithium phthalocyanine thin films: Part I. Structure and morphology M. Brinkmann, S. Graff, C. Chaumont, J-J. André

Fracture toughness of diamondlike carbon coatings M. Nastasi, P. Kodali, K.C. Walter, J.D. Embury, R. Raj, Y. Nakamura

Microstructure modification of amorphous carbon films by ion-implantation techniques

B. Wei, K. Komvopoulos, I.G. Brown

ABSTRACTS

Subsolidus phase equilibria in the La₂O₃-CeO₂-Co₂O₃ system M. Hrovat, J. Holc, S. Bernik

(Jožef Stefan Institute)

Subsolidus equilibria in air in the La_2O_3 -CeO₂-Co₂O₃ system were studied with the aim to obtain information on possible interactions between $LaCoO_3$ based cathode and CeO2-based solid electrolyte in solid oxide fuel cells (SOFC). No ternary compound was found. The tie line is between LaCoO3 and CeO2 Order No.: JA905-005 © 1999 MRS

ARTICLES

Effect of P_{O2} and Ag on the phase formation of the Bi(Pb)-2223 superconductor

W. Wong-Ng,¹ L.P. Cook,¹ W. Greenwood^{1,2}

(¹National Institute of Standards and Technology, ²University of Maryland) The chemical reactions and the compositional characteristics of liquids which lead to the phase formation of the Bi(Pb)-2223 [(Bi,Pb) : Sr : Ca : Cu : O] superconductor have been studied for a precursor composition of $Bi_{1.8}Pb_{0.4}Sr_2Ca_{2.2}Cu_3O_x$. The combined techniques of quenching, powder. xray diffraction, differential thermal/thermogravimetric analysis (DTA/TGA), scanning electron microscopy (SEM), and energy dispersive x-ray spectroscopy (EDS) were used to characterize the subsolidus phases and the presence of liquid. Samples were annealed under purified air and under a volume fraction mixture of 7.5% O₂/92.5% Ar. The effects of Ag in both the pure air and the 7.5% O2/92.5% Ar experiments were also studied. Results are discussed with respect to their processing implications. Order No.: JA905-006

© 1999 MRS

Entrapment of elongated and crystallographically aligned pores in YBa2Cu3O7-y melt-textured with BaCeO3 addition

C-J. Kim, G-W. Hong, S-J.L. Kang2 (¹Korea Atomic Energy Research Institute,

²Korea Advanced Institute of Science and Technology)

Compared to entrapped spherical pores in YBa2Cu3O7-y (123) crystals melt-textured without additives, the pores entrapped within 123 crystals melttextured with 5 wt% BaCeO3 are elongated and aligned parallel to (100), (010), and (001) growth planes of the 123 crystals. The front side of the pores that meets first the growth front of the 123 crystal is faceted, but the backside is wavy. Many BaCeO3 particles are segregated at the wavy surface. The crystallographic alignment of the elongated pores and the segregation of BaCeO₃ particles are discussed in terms of the contact angle of the pores on the growth front and interfacial energy relationships between the related phases © 1999 MRS Order No.: JA905-007

Texture analysis and microstructural features in YBa2Cu3O6+x zone-partial-melted samples with Y2BaCuO5 additions R. Cabré,¹ E. Martínez,² Jna. Gavaldà,¹ R. Solé,¹ J. Massons,¹ C. Rillo,²

M. Aguiló,1 F. Díaz1

(¹Universitat Rovira i Virgili, ²Universidad de Zaragoza)

Rod-shaped samples of $YBa_2Cu_3O_{6+x}$ (Y123) with different contents of Y_2BaCuO_5 (Y211) are textured by the partial-zone melting method in order to produce single-domain specimens. The microstructure and magnetic properties of the samples are analyzed as a function of the Y211 initial addition. Y211 precipitates are more homogeneously distributed and smaller, and the superconducting properties of the sample also improve, so when the initial content of Y211 increases, J_c values are high. Texture analysis is carried out by the xray pole figure technique. Order No.: JA905-008

© 1999 MRS

Effects of inorganic components on the mechanical properties of inorganic-organic hybrids synthesized from metal alkoxides and polydimethylsiloxane

N. Yamada, I. Yoshinaga, S. Katayama

(Nippon Steel Corporation)

Inorganic-organic hybrids (M-O-PDMS hybrids) have been synthesized from silanol-terminated polydimethylsiloxane (PDMS) and inorganic sources of Al(O-sec-C₄H₉)₃, Ti(OC₂H₅)₄ and Ta(OC₂H₅)₅. The molar ratio of M(OR)_{n'}</sub> PDMS and the inorganic component derived from the different metal alkox ides were found to influence the structure and mechanical properties of the hybrids. Differential scanning calorimetry (DSC) measurements showed that the interaction between the inorganic component and PDMS increased in the order AI-O-PDMS < Ta-O-PDMS < Ti-O-PDMS hybrid. The stress-strain experiments revealed that the mechanical properties of the M-O-PDMS hybrids differed by the inorganic component reflecting the network structure and strength of the interaction between the inorganic component and PDMS. © 1999 MRS Order No.: JA905-009

Promotion of phase transformation and single-phase formation in silver-doped TI-Ba-Ca-Cu-O superconducting thin films H-S. Koo, T-Y. Tseng

(National Chiao-Tung University)

Phase transformation and physical characteristics of the spray-pyrolyzed Tl-Ba-Ca-Cu-O superconducting films with 3 mol% silver dopant have been studied using electrical resistivity, x-ray diffraction, and scanning electron microscopy. The major phase formed in the resultant film, annealed at a temperature of 885 °C for 3 min, was found to be the nearly single-phase, high-T_c $Tl_2Ba_2Ca_2Cu_3O_v$ (TI-2223). The multiple phase of $Tl_2Ba_2Ca_2Cu_3O_v$ and TIBa2Ca2Cu3Oy (TI-1223) appeared at annealing temperatures lower and higher than 885 °C. It was also observed that Ag dopant effectively reduces normal resistivity at 300 K and enhances the phase transformation of single-Tl-layer TI-1223 to double-TI-layer TI-2223 phases and further helps to form the nearly single-phase TI-2223 within short duration. Critical transition temperature ($T_{c, zero}$) and current density (J_c , 77K, 0Tesla) of the best resultant film were shown to be 123 K and 5.7 × 10⁴ A/cm², respectively. Order No.: JA905-010 © 1999 MRS

A study of the dislocations in Si-doped GaAs comparing diluted Sirtl light-etching, electron-beam-induced current, and micro-Raman techniques

P. Martin,¹ J. Jiménez,¹ C. Frigeri,² L.F. Sanz,¹ J.L. Weyher³ ¹ETS Ingenieros Industriales, ²CNR-MASPEC Institute,

³Polish Academy of Sciences U. Sokolowska)

Impurity atmospheres around dislocations have been studied in n-type Sidoped liquid encapsulated Czochralski (LEC) GaAs substrates by micro-Raman spectroscopy, diluted Sirtl-like etching with light (DSL) method and electronbeam-induced current (EBIC). A complete morphological study of the recombinative atmospheres revealed by photoetching was achieved by phase stepping microscopy (PSM), which is an optical interferometry technique allowing the obtainment of the surface topography with a high vertical solution (in the nanometer range). The minority carrier diffusion length was measured by EBIC at different points of the atmospheres. Structural distortion at the regions surrounding the dislocation core were observed by micro-Raman spectroscopy. The carrier depletion depth and the recombination of the photogenerated carriers were also studied by Raman spectroscopy, obtaining a good agreement with the EBIC data and the photoetching rates. Impurity gettering and diffusion and defect reactions involving As interstitials are assumed to play a major role in the formation of the recombinative atmospheres. Order No.: JA905-011 © 1999 MRS

High-resolution x-ray diffraction study of In_{0.25}Ga_{0.75}Sb/InAs superlattice

A. Vigliante, H. Homma, J.T. Zborowski, T.D. Golding, S.C. Moss (University of Houston)

A $In_{0.25}Ga_{0.75}Sb/InAs$ strained-layer superlattice, grown by molecular-beam epitaxy (MBE) on a GaSb[001] substrate, has been characterized by four-circle x-ray diffractometry. This system, proposed by Maliot and Smith for ir detection application, is challenging because of the two group V species and the likelihood of cross-incorporation of the different elements during growth, leading possibly to interdiffusion and thus to a more diffuse interface. High-resolution x-ray diffraction (XRD) profiles were obtained about several reciprocal lattice points in order to extract a reliable set of structural parameters. The profiles were then successfully modeled by computer simulation. The presence of many sharp higher-order satellite reflections in the XRD pro-

files is a measure of the high quality of the superlattices. The normal and lateral structural coherence was also measured and will be discussed. Order No.: JA905-012 © 1999 MRS

Temperature and porosity dependence of the thermoelectric properties of SiC/Ag sintered materials

K. Kato, K. Asai, Y. Okamoto, J. Morimoto, T. Miyakawa (National Defense Academy)

We have studied the thermoelectric properties of SiC-based thermoelectric semiconductor with Ag and polysilastylene (PSS) as a dopant and as a sintering additive, respectively. Ag is an effective dopant to decrease the electrical resistivity of the SiC-based p-type thermoelectric semiconductor. It introduces carrier (hole) concentration 10^{3} -10⁴ times larger than the case of Al-doped SiC with the typical doping concentration. PSS can control the sample density, which is one of the important factors in decreasing the electrical resistivity and thermal conductivity of the sintered samples. The figure of merit of the sample with Ag 2.0 wt% and PSS 0.1 wt% was estimated to reach 4 × 10⁻⁴ K⁻¹ at 700 ℃. This value implies that the SiC/Ag system is one of the promising thermoelectric materials for high-temperature region. Order No.: JA905-013 © 1999 MRS

Synthesis of Fe-rich Fe-Al nanocrystalline solid solutions using ball milling

H.G. Jiang, H.M. Hu, E.J. Lavernia (University of California-Irvine)

The synthesis of nanocrystalline Fe, Fe-4 wt% Al and Fe-10 wt% Al solid solutions by SPEX ball milling has been studied. The microstructural evolution during ball milling, as well as subsequent heat treatment, has been characterized. The results demonstrate that ball milling promotes the formation of aFe-4 wt% Al and aFe-10 wt% Al solid solutions by reducing the activation energy of these alloys and generating thermal energy during this process. For Fe-10 wt% Al powders milled for various time intervals up to approximately 20 minutes, the FeAl intermetallic compound is formed. For alloys annealed at temperatures ranging from 600 to 1000 °C, the addition of 10 wt% Al to Fe significantly enhances the thermal stability of the nanocrystalline Fe-Al alloys. Interestingly, the addition of Al within the range of 4-10 wt% seems to have little effect on the thermal stability of these alloys annealed under the same conditions. Also, the thermal stability improves for alloys milled in air, as opposed to those processed using Ar.

Order No.: JA905-014

© 1999 MRS

Solidification of undercooled molten Cu₃₀Ni₇₀

J.Z. Xiao, H.W. Kui

(The Chinese University of Hong Kong) Recently, it was demonstrated that grain refinement in undercooled Cu30Ni70 is brought about by a remelting of those initially formed dendrites (termed novel dendrites) which are unstable against melting. Also, it was found that in the same transition regime, there is a sharp drop in the specific volume of the undercooled specimens. Before entering into the transition regime, the novel dendrites found in an undercooled specimen are arranged in a regular pattern and the microstructures consist of large dendrites. Voids are found mainly at the dendritic spacings of the large dendrites. On the other hand, near the upper end of the transition regime, the microstructures consist of equiaxed refined grains. Furthermore, each of these grains contains a novel dendrite. Voids have moved to the interdendritic or grain boundaries. Based on these observations, a solidification mechanism of undercooled molten Cu30Ni70 is proposed. Order No.: JA905-015

© 1999 MRS

Characterization of Fe–Ni(C) nanocapsules synthesized by arc discharge in methane

X.L. Dong, 1,2 Z.D. Zhang, 1 S.R. Jin, 2 W.M. Sun, 2 X.G. Zhao, 1 Z.J. Li, 2 Y.C. Chuang¹

(¹Academia Sinica, ²Shenyang Polytechnic University)

Ultrafine Fe-Ni(C) particles of various composition were prepared by arc discharge synthesis in a methane atmosphere. The particles were characterized by x-ray diffraction, transmission electron microscopy, energy disperse spec troscopy, chemical analysis, x-ray photoelectron spectroscopy, Mössbauer spectroscopy, and magnetization measurement. The carbon atoms solubilizing at interstitial sites in y-(Fe, Ni, C) solution particles have the effects of forming austenite structure and changing microstructures as well as magnetic properties. A carbon layer covers the surface of Fe-Ni(C) particles to form the nanocapsules and protect them from oxidization. The mechanism of forming Fe-Ni(C) nanocapsules in the methane atmosphere was analyzed Order No.: JA905-016 © 1999 MRS

Prediction of new additives for galvanizing process by the properties of their constituent chemical elements H.M. Jin,1 Y. Li,1 P. Wu2

(¹National University of Singapore, ²Institute of High Performance Computing) Chemical element properties are generally classified in six groups: size, atomic number, electrochemical factor, valence electron, cohesive energy, and angular valence orbital. It is well known that some bulk properties of materials, like electrical conductivity and heat capacity of metals, may be interpreted in principle based on their constituent chemical element properties. In this study, effects of additives in galvanizing have been correlated to the chemical element properties of the additives. By screening all chemical elements (in the periodic table of elements) with this model, new additives, like Ca, Sc, Ge, Sr, and Y, have been predicted to reduce the steel weight loss in galvanizing. This model may also help to design new alloys as additives. Order No.: JA905-017 © 1999 MRS

Piezoelectric and pyroelectric behavior of lead zirconate titanate-lead sulphide-glass nanocomposites

T.K. Kundu,¹ D. Chakravorty,¹ L.E. Cross²

(¹Indian Association for the Cultivation of Science, ²Pennsylvania State University)

Composites containing micron-sized lead zirconate titanate and nanometersized lead sulphide in a glass matrix were prepared using a sol-gel technique. The PbS size ranged from 3.5 to 15.3 nm. It was possible to pole some of these nanocomposites. The measured values of saturation polarization, remanent polarization, and coercive field showed an increase as the PbS particle size was enhanced. The composites exhibited improvement in the piezoelectric and pyroelectric behavior as compared to that of the base glass-ceramic. Order No.: JA905-018

© 1999 MRS

A new method for the production of a molybdenum-zirconia cermet C.M. Lukaniuk, L.D. Schwartz, T.H. Etsell

(University of Alberta)

A novel method was studied for producing a ceramic-metal matrix composite (cermet) of Mo metal and zirconia powder. The first step was to precipitate dissolved molybdenum from solution onto activated zirconia powder. The molybdenum plated out on the zirconia as molybdenum hydroxide. Next, the coated powders were heated in a tube furnace under hydrogen gas to reduce the molybdenum hydroxide to metallic molybdenum. Finally, the powders were pressed and sintered into cermet pellets. The Mo coatings were 1.5 to 4.2 µm thick and very uniform, enabling the particles to be sintered together. The sintered pellets had superb electrical conductivity (less than 1 ohm of resistance). Order No.: JA905-019 © 1999 MRS

Chemical synthesis and characterization of polyaniline-molybdenum trisulfide composite

F. Fusalba, D. Bélanger

(Université du Québec à Montréal)

A novel polyaniline-molybdenum trisulfide composite has been prepared by chemical polymerization from an acidic (1 M HCl) aqueous solution containing aniline and ammonium tetrathiomolybdate. The presence of molybdenum trisulfide in the polyaniline matrix induces morphological change to the polymer as evidenced by scanning electron micrographs, X-ray diffraction and differential scanning calorimetry indicate that polyaniline-molybdenum trisulfide is slightly less crystalline than polyaniline-HCl. X-ray photoelectron spectroscopy (XPS) and elemental analysis have been used to confirm the presence of molybdenum trisulfide in the polymer matrix. The XPS data also confirm that molybdenum trisulfide and tetrathiomolybdate anions are present with polyaniline to form a new inorganic-organic composite. Order No.: JA905-020 © 1999 MRS

The effects of nonhydrostatic compression and applied electric field on the electromechanical behavior of poled lead zirconate titanate 95/5-2Nb ceramic during the rhombohedral to antiferroelectric polymorphic transformation

D.H. Zeuch, S.T. Montgomery, D.J. Holcomb

(Sandia National Laboratories)

We conducted hydrostatic compression and constant-stress-difference experiments, with and without an applied electric field, on poled, niobium-doped lead zirconate titanate ceramic. The objective was to quantify the effects of nonhydrostatic stress and electric field bias on electromechanical behavior of the ceramic

during the ferroelectric, rhombohedral -> antiferroelectric, orthorhombic phase transformation. Increasing stress difference (shear stress) decreases the mean stress at which the transformation occurs. Increasing shear stress also retards the rate of transformation, causing reductions in both the rate of charge release and peak voltage attained during depoling. Application of the electric field bias slightly increases the transformation pressure for poled ceramic. Previously, we showed that under nonhydrostatic stress, the transformation took place in unpoled ceramic when the maximum compressive stress equalled the hydrostatic pressure at which the transformation would otherwise occur. This simple stress criterion does not apply to poled ceramic. However, poled material has a preferred crystallographic orientation and mechanical anisotropy, whereas unpoled ceramic is isotropic. We present a qualitative model for the transformation under nonhydrostatic stress, related to that anisotropy, which resolves these seemingly disparate observations. Order No.: JA905-021 © 1999 MRS

Synthesis of anorthite by the Pechini process and structural investigation of the hexagonal phase

S-H. Hong, J.F. Young, P. Yu, R.J. Kirkpatrick

(University of Illinois at Urbana Champaign)

Stoichiometric CaAl₂Si₂O₈ gels prepared by the Pechini process crystallize to triclinic anorthite via an intermediate, previously unknown pseudohexagonal phase. Hydrothermal treatment of this pseudohexagonal phase at 350 °C transforms it to hexagonal anorthite. These combined processes produce the hexagonal phase via a low-temperature, chemical route in contrast to the conventional high-temperature melting and crystallization method. Powder x-ray diffraction data and nuclear magnetic resonance (NMR) spectra of the hexagonal anorthite agree well with the published structure. They indicate a high degree of tetrahedral Si/Al ordering within the layers, but long-range disorder in the average structure due to (001) stacking faults present between the layers. Order No.: JA905-022 © 1999 MRS

Calorimetric and high-resolution transmission electron microscopy study of nanocrystallization in zirconia gel J. Málek, T. Mitsuhashi, J. Ramírez-Castellanos, Y. Matsui

(National Institute for Research in Inorganic Materials) The formation of metastable tetragonal zirconia nanophase by thermal

treatment of a zirconia gel derived from zirconyl chloride has been studied by high-resolution transmission electron microscopy (HRTEM) and differential scanning calorimetry (DSC). HRTEM observations revealed that a fully crystallized sample consists of nanocrystals, around 13 nm in size. This nanocrystalline t-ZrO2 has practically the same crystal structure as that of the high-temperature tetragonal zirconia phase. The nonisothermal crystallization rate is very fast in as-prepared zirconia gel. DSC data at various heating rates can be described by a two parameter model which predicts the crystallization kinetics in isothermal conditions very well. The Johnson-Mehl-Avrami (JMA) model can be used, however, in partially crystalline samples (crystallinity >30%) where the rate of crystallization process is considerably slower. The kinetic exponent of the JMA model ($m = 1.0 \pm 0.1$) then corresponds to linear dependence of the crystallization rate as a function of the fraction crystallized. Order No.: JA905-023 © 1999 MRS

Morphological evolution of barium titanate synthesized in water in the presence of polymeric species

R.B. Bagwell, J. Sindel, W. Sigmund

(Max-Planck-Institut für Metallforschung and Universität Stuttgart)

The synthesis of barium titanate (BaTiO₃) was investigated in water at 90 °C in the presence of polymeric additives. Homopolymers (PAA) and block copolymers (PEO/PMAA) were added during synthesis to influence particle morphology and size distribution. The polymers affected the morphological evolution of the forming powder by adsorbing preferentially on specific planes. The polymeric species also slowed the formation of barium titanate. The barium concentration also changed the morphology, particle size, and other powder characteristics. Order No.: JA905-024 © 1999 MRS

Characterization of sol-gel $Pb(Zr_{0.53}Ti_{0.47})O_3$ in the thickness range 0.25-10 um

R. Kurchania, S.J. Milne

(University of Leeds)

Films of nominal composition $Pb(Zr_{0.53}Ti_{0.47})O_3$ (PZT) in the thickness range 0.25-10 µm have been fabricated on Pt/Ti/SiO2/Si substrates using a propanediol-based sol-gel route. The spun-on coatings were prefired at 350 and 600 °C between successive depositions before firing the multilayer stack at 700 °C for 15 min. The variations in crystallite orientation, microstructure, and dielectric and ferroelectric properties were determined as a function of film thickness. For a constant applied field of 150 kV cm⁻¹, remanent polarization decreased progressively from 35 to 17 μ C cm⁻² as film thickness decreased in the range 10-0.25 µm; values of coercive field were reasonably constant, 18-19 kV cm⁻¹, for films between 2 and 10 µm, but increased sharply below 2 μ m, reaching 46 kV cm⁻¹ for a 0.25 μ m film. Relative permittivity (ε_r) decreased from about 1400 to about 940 with most of the reduction occurring in films less than 2 µm in thickness. These trends are discussed in terms of the presumed influence of interfacial phenomena on the measured electrical response. Order No.: JA905-025 © 1999 MRS

Properties of BaBi₂Ta₂O₉ thin films prepared by chemical solution deposition technique for dynamic random-access memory applications

C.R. Foschini,¹ P.C. Joshi,¹ J.A. Varela,² S.B. Desu¹

(¹Virginia Tech, ²Universidade Estadual Paulista)

We report on the properties of BaBi2Ta2O9 (BBT) thin films for dynamic random-access memory (DRAM) and integrated capacitor applications. Crystalline BBT thin films were successfully fabricated by chemical solution deposition technique on Pt-coated Si substrates at a low annealing temperature of 650 °C. The films were characterized in terms of structural, dielectric, and insulating properties. The electrical measurements were conducted on Pt/BBT/Pt capacitors. The typical measured small signal dielectric constant and dissipation factor, at 100 KHz, were 282 and 0.023, respectively, for films annealed at 700 °C for 60 min. The leakage current density of the films was lower than 10-9 A/cm² at an applied electric field of 300 kV/cm. A charge storage density of 38.4 fC/µm² was obtained at an applied electric field of 200 kV/cm. The high dielectric constant, low dielectric loss, and low leakage current density suggest the suitability of BBT thin films as dielectric layer for DRAM and integrated capacitor applications. © 1999 MRS Order No.: JA905-026

Structure and growth of yttrium iron garnet thin films with enhanced magnetic properties by metalorganic chemical vapor deposition

V.N. Moorthy,¹ S. Dhara,¹ A.C. Rastogi,¹ B.K. Das,¹ D.V.S. Jain² (¹National Physical Laboratory, ²Punjab University)

Growth of undoped and Co/Ce-doped yttrium iron garnet films by a lowpressure metalorganic chemical vapor deposition (MOCVD) process is described. As-deposited films require a 900 °C oxygen anneal to crystallize into the cubic garnet phase. Inclusion of secondary nonmagnetic phases in the films is attributed to the local deviations in the Y/Fe oxide ratios. Crystallization behavior as established by x-ray diffraction studies shows that the garnet phase formation occurs by two mechanisms---by solid phase reaction of Y2O3 and α -Fe₂O₃ and by transformation of hex-YFeO₃ solid solution with Fe₂O₃. Garnet film growth by CVD occurs by precursor pyrolysis in the gas phase and by interaction with the substrate through a complex reaction sequence described through a model. Magnetic studies of undoped and Co/Ce-doped films show enhancement in perpendicular anisotropy and extremely high coercivity values of 170 kA/m (= 2125 Oe) and saturation magnetization of 104 kA/m $(4\pi M_s = 1306 \text{ Gs})$ due to Co/Ce-doping which also promotes the garnet phase crystallization.

Order No.: JA905-027

© 1999 MRS

Planar defects in ZnO thin films deposited on optical fibers and flat substrates

L. Sagalowicz, G.R. Fox

(EPFL)

The microstructure and the defects of ZnO coatings deposited at room temperature by sputtering onto fibers and flat substrates were characterized using transmission electron microscopy (TEM), scanning electron microscopy, and x-ray diffraction (XRD). XRD shows that the films have an [0001] preferred orientation and a large angular width of the 0002 reflection. According to TEM observations, the film microstructure consists of columnar grains, which contain large concentrations of basal planar defects, and dislocations. High-resolution transmission electron microscopy analysis and the associated image simulation are in full agreement with the presence of single and double stacking faults. The relation between the observed defects and the 0002 peak broadening is discussed. © 1999 MRS Order No.: JA905-028

Si₃N₄-SiC-Y₂O₃ ceramics derived from vttrium-modified block copolymer of perhydropolysilazane and hydroxy-polycarbosilane Y. Iwamoto,¹ K. Kikuta,² S. Hirano²

(¹Synergy Ceramics Laboratory, ²Nagoya University)

A polymeric precursor for Si₃N₄-SiC-Y₂O₃ ceramic system was synthesized by block copolymerization of perhydropolysilazane (PHPS) with hydroxy-polycarbosilane (PCS-OH), followed by chemical modification with yttrium methoxide. Fully dense Si₃N₄-SiC-Y₂O₃ ceramics were successfully synthesized by pyrolysis of the polymeric precursor at 1000 °C, followed by hot pressing at 1800 °C in N₂. The resulting ceramics revealed that β -SiC particles were dispersed in a size range of about 10 to 600 nm, and a large amount of β -SiC submicron particles were segregated at the β -Si₃N₄ matrix grain boundaries. It was found that the yttrium-modified block copolymer of PHPS and PCS-OH yielded rather unique binary ceramics composed of β -SiC-Y₂O₃ and β-SiC nanoparticle-dispersed Si₃N₄-Y₂O₃. © 1999 MRS Order No.: JA905-029

Residual stress fields in sol-gel derived thin TiO₂ layers

D.H.J. Teeuw, M. de Haas, J.Th.M. De Hosson

(University of Groningen)

This paper discusses the induction of residual stresses during the curing process of thin titania layers, which are derived using a sol-gel process. During this process, stresses may build up in the spinning stage, the drying stage, and the consolidation stage. The magnitude and character of these stresses depend heavily on the morphology of the layers in the various stages and the processing conditions. Dried layers are densified using two different processes, conventional furnace heating and laser heating. X-ray analysis and scanning electron microscopy are used as tools to study crystallization, grain growth, phase transformation, and the evolution of residual stress fields in the thin titania layers. Through an extensive study of the residual stress state in the layers, more insight is gained in the evolution of stresses during the curing process of sol-gel derived thin titania layers Order No.: JA905-030 © 1999 MRS

Microstructural evolution and mechanical properties of gas-pressure-sintered Si₃N₄ with Yb₂O₃ as a sintering aid

K-M. Lee, W-H. Lee, Y-H. Koh, J-J. Choi, H-E. Kim, S.S. Baek² (¹Seoul National University, ²Agency for Defense Development)

Microstructural evolution and mechanical properties of gas-pressure-sintered Si₃N₄ with 4 wt% Yb₂O₃ as a sintering aid were investigated. The microstructure was not uniform throughout the specimen. Extremely large elongated grains were formed at the outer region near the surface, while relatively small elongated grains were formed at the inner region of the specimen. The outer region expanded inward with the sintering time. Mechanical properties, such as flexural strength, fracture toughness, and R-curve behavior of the specimens were strongly influenced by these variations in microstructure. The fracture toughness and the Rcurve behavior of the outer region were higher than those of the inner region of the same specimen. On the other hand, the strength of the inner region was higher than that of the outer region. By controlling the relative thickness of each region, Si₃N₄ specimens having functionally graded microstructure were obtained. The Si₃N₄ with such microstructure exhibited high strength, high fracture toughness, and good flaw tolerance at the same time. Order No.: JA905-031 © 1999 MRS

Experimental assessment of the inhibition of reduction of Ca²⁺-doped barium titanate in a reducing atmosphere T-T. Fang, J-T. Shuei

(National Cheng Kung University)

Several experiments have been conducted to assess the possible mechanisms for the inhibition of reduction of Ca2+-doped barium titanate in a reducing atmosphere. Three methods, i.e., conventional, semiwet, and citrate processes, have been used to prepare the powders. It was found that the formation mechanism would influence the occupation of Ca2+ in the B site. Moreover, it was concluded that Ca2+ occupation of the B site is the major cause for the inhibition of reduction of Ca2+-doped barium titanate. Ti deficiency would be the driving force for Ca²⁺ to occupy the B site. Order No.: JA905-032 © 1999 MRS

The effect of Zn(OH)₂ addition on the electrode properties of nickel hydroxide electrodes

J. Chen, D.H. Bradhurst, S.X. Dou, H.K. Liu

(University of Wollongong)

Nickel hydroxide powders currently used in the positive electrode of nickelmetal hydride (Ni-MH) batteries require cobalt or cobalt oxides to make them viable and attractive. As a step to eliminate the cobalt-containing materials,

spherical nickel hydroxide powders coprecipitated with Zn(OH)₂ were prepared by a spraying technique. These powders, which have a higher tapping density and a much smaller pore volume than conventional powders, were used as the active materials of nickel hydroxide electrodes. The effects of the Zn(OH)2 additions on the electrode properties, such as percentage utilization and cycle life, were studied, and the relationship between the electrode performance and the formation of γ -NiOOH was investigated. The cycle life was increased because there was less electrode swelling due to much reduced formation of γ -NiOOH. Order No.: JA905-033

© 1999 MRS

Synthesis and luminescence of the nanosized Ce-doped silica particles dispersed within the pores of mesoporous silica host W. Cai,^{1,2} Y. Zhang,¹ L. Zhang^{1,2}

(¹Academia Sinica, ²University of Science and Technology of China)

Nanosized Ce-doped silica particles (without and with Al addition) dispersed within pores of mesoporous silica host were synthesized by soaking and sol-gel technique. It was found that the dispersed phosphor particles are mainly located within the pores that are less than 4 nm in diameter. There exist two luminescence peaks at about 350 and 700 nm, respectively, for this phosphor in the dispersed or aggregated state. For the dispersed system, the luminescence intensities of both peaks are more than 14 times higher than those of the aggregated one, the shoulders on the lower sides of the luminescence peaks disappear, and no effect of Al addition on the luminescence occurs which is in contrast to the aggregated system. This is mainly attributed to the high dispersity of nanosized phosphor particles in the host and the effective avoidance of a clustering of Ce3+ ions. Order No.: JA905-034 © 1999 MRS

A self-propagating high-temperature synthesis method for synthesis of AIN powder

S-L. Chung, W-L. Yu, C-N. Lin

(National Cheng Kung University)

A new self-propagating high-temperature synthesis (SHS) process has been developed for synthesis of AIN powder under low nitrogen pressures. AI and NH_4X (X = F, Cl, Br, or I) powders were mixed and pressed into a compact, which was placed in a reaction chamber filled with nitrogen. The combustion synthesis reaction was ignited by heating directly the compact, and high product yields (~90%) were obtained under nitrogen pressures of around 0.5 MPa. The product yield was affected by the reactant composition, the nitrogen pressure, and the compact-forming pressure. The powder as synthesized consists mainly of fibers, coarse granules, and agglomerated fine particles, which become mostly smaller than 10 µm after grinding. A reaction process was also proposed that explains the effects of the experimental parameters on the product yield. Order No.: JA905-035 © 1999 MRS

Synthesis of amorphous boron nitride from the molecular precursor ammonia-monochloroborane

D.R. Ketchum, A.L. DeGraffenreid, P.M. Niedenzu, S.G. Shore (The Ohio State University)

Ammonia-monochloroborane, NH3BH2Cl, has been synthesized from the reaction of ammonia-borane with HCl in Et₂O. Decomposition of the solid under NH3 to 600 °C produced amorphous BN in 97% yield. The ¹¹B magic angle spinning (MAS) nuclear magnetic resonance (NMR) spectrum of the amorphous BN is indicative of boron in the same environment as in hexagonal BN. Subsequent pyrolysis of the amorphous BN to 1000 °C led to the formation of turbostratic BN as confirmed by x-ray diffraction (XRD) analysis. Gas evolution during this pyrolysis confirmed that the precursor loses H₂ and HCl. Order No.: JA905-036 © 1999 MRS

Fabrication of undoped near-monophase Ba₂Ti₉O₂₀ via rapid thermal processing

W. Lin, R.F. Speyer

(Georgia Institute of Technology)

Rapid thermal processing of BaTiO₉ and TiO₂ pressed powders at 500 °C/min to 1250 °C for 2 h in an infrared furnace resulted in a mixture of Ba2Ti9O20, BaTi₄O₉, and TiO₂. Further heat treatment at 1390 °C led to 96 vol% phasepure Ba2Ti9O20 from an initial mixture devoid of any dopant. Heat treatment at rates decreasing to 5 °C/min facilitated agglomeration of TiO2. This, in turn, increased the diffusion distance required for reaction of BaTi₄O₉ and TiO₂ to form Ba2Ti9O20. Order No.: JA905-037

© 1999 MRS

Microstructure and thermokinetics analysis of CS AIN K, Chen,¹ C, Ge,² J, Li,² W, Cao²

(¹Tsinghua University, ²University of Science and Technology Beijing) The mechanism for combustion synthesis (CS) of AIN was investigated in the present paper. A novel quenching technique was developed to retain the high-temperature structure formed in the sample during the combustion process. Based on the microstructure observation of the quenched specimen and thermodynamic analysis, a two-step reaction mechanism for CS AlN, i.e., vaporization of Al and subsequent reaction with N2, is proposed. Order No.: JA905-038

© 1999 MRS

Modeling studies of the effect of thermal and electrical conductivities and relative density on field-activated self-propagating combustion synthesis

E.M. Carrillo-Heian, O.A. Graeve, A. Feng, J.A. Faghih, Z.A. Munir (University of California-Davis)

The role of the electrical conductivity of the product and of the thermal conductivities of the reactants on self-propagating combustion synthesis was investigated through modeling studies. Similar studies were made to investigate the role of the relative density of the reactants. The effect of an imposed electric field on the results of the modeling analysis was considered. For any given imposed field, the wave velocity exhibited a maximum at a given normalized thermal conductivity, electrical conductivity, and relative density. The results are discussed in terms of the Joule heat contribution of the field and are compared with experimental observations. Order No.: JA905-039

© 1999 MRS

Silicon nitride:

Enthalpy of formation of the α - and β -polymorphs and the effect of C and O impurties

J. Liang,¹ L. Topor,¹ A. Navrotsky,¹ M. Mitomo² (¹University of California—Davis,

²National Institute of Research in Inorganic Materials)

High-temperature oxidative drop solution calorimetry was used to measure the enthalpy of formation of α - and β -Si₃N₄. Two different solvents, molten alkali borate (48 wt% LiBO2-52 wt% NaBO2) at 1043 and 1073 K and potassium vanadate (K₂O • 3V₂O₅) at 973 K, were used, giving the same results. Pure α and β -Si₃N₄ polymorphs have the same molar enthalpy of formation at 298 K of -850.9 ± 22.4 and -852.0 ± 8.7 kJ/mol, respectively. The unit cell dimensions of impure α -Si₃N₄ samples depend linearly on the O and C impurity contents, and so does the molar enthalpy of formation. The energetic stability of the α -Si₃N₄ phase decreases when the sample contains O and C impurities. The experimental evidence strongly suggests that the impurities dissolve into the α -Si₃N₄ structure to form a (limited) isostructural solid solution series but that this solid solution series is energetically less stable than a mechanical mixture of pure (α or β) Si₃N₄, SiO₂, and SiC. Thus, the α-phase is not stabilized by impurities and is probably always metastable. Order No.: JA905-040 © 1999 MRS

Structural characterization of deuterated titanium thin films R. Checchetto, P. Scardi

(Università di Trento)

Pure and deuterated titanium thin films 140 nm thick were deposited on <100> Si wafers by electron beam evaporation, keeping the substrate temperature at 150, 300, and 450 °C. Pure Ti samples were deposited in a high vacuum condition while, for deuterated samples, deuterium high-purity gas was intro duced in the deposition chamber during the process. Film composition was studied by Rutherford backscattering spectroscopy (RBS) and elastic recoil detection analysis (ERDA), whereas structural characterization of the deposited layers was carried out by x-ray diffraction (XRD) using both the traditional Bragg-Brentano geometry and a parallel beam setup for pole figure measurements. Titantium films deposited in a high vacuum showed the hexagonal Ti structure (α -Ti) and grew with a double orientation at each of the examined substrate temperatures. Deuterated titanium films deposited at 105 °C had a compositional ratio Ti : D = 1 : 0.35 and grew with a [111] oriented fcc structure, suggesting the formation at low temperature of a substoichiometric δ hydride phase. Deuterated films deposited at higher substrate temperatures revealed a lower deuterium content and XRD reflections corresponding to the hexagonal Ti phase. The present results were interpreted according to a temperature-dependent D2 adsorption mechanism at the surface of the continuously growing Ti film. Order No.: JA905-041 © 1999 MRS

MRS BULLETIN/MARCH 1999

Face-centered-cubic titanium: An artifact in titanium/aluminum multilayers

J. Bonevich,¹ D. van Heerden,² D. Josell¹ (¹National Institute of Standards and Technology, ²The Johns Hopkins University)

The present investigation is the first comprehensive comparative study of x-ray diffraction (XRD) and transmission electron microscopy (TEM) results to address the important issue of fcc Ti formation in nanoscale multilayers. Ti/Al multilayers with 7.2 and 5.2 nm composition modulation wavelengths were studied by reflection and transmission XRD, as well as transmission electron diffraction (ED), high-resolution TEM, and energy-filtered TEM. Previous reports have claimed deposition of fcc Ti in multilayer systems. Our results demonstrate that the Ti in Ti/Al multilayers deposits in the hcp form and that fcc Ti is merely an artifact of producing specimens for cross-sectional TEM. Order No.: JA905-042 © 1999 MRS

Programmed substrate temperature ramping to increase nucleation density and decrease surface roughness during metalorganic chemical vapor deposition of aluminum

R. Jonnalagadda,¹ D. Yang,² B.R. Rogers,³ J.T. Hillman,⁴ R.F. Foster,⁴ T.S. Cale² (¹Allied Signal, Inc., ²Rensselaer Polytechnic Institute, ³Vanderbilt University, ⁴Tokvo Electron Arizona)

We discuss substrate temperature ramping effects during chemical vapor deposition of aluminum on nucleation density, texture, surface roughness, and resistivity of the resulting films. Results from three different process protocols are presented. Ramping the temperature down during the deposition from 673 K resulted in a larger fraction of small nuclei compared to deposition at a constant temperature of 573 K. From among the protocols studied, the lowest surface roughness was obtained by initially depositing for a short time while ramping the temperature down from 673 K, followed by deposition at 573 K, compared to all the other films. The same process protocol resulted in the highest Al(111) texturing, highest reflectivity, and lowest resistivity. Order No.: JA905-043

© 1999 MRS

Corrosion performance of ferrous and refractory metals in molten salts under reducing conditions

J.E. Indacochea, J.L. Smith K.R. Litko, E.J. Karell

(Argonne National Laboratory)

A lithium reduction technique to condition spent fuel for disposal has been developed at the Argonne National Laboratory. There is a need to ensure adequate vessel longevity through corrosion testing and, if necessary, materials development. Several ferrous alloys and tantalum specimens were submitted to a corrosion test at 725 °C for thirty days in an argon atmosphere, using a lithiumchloride salt saturated with lithium metal and containing small amounts of lithium oxide and lithium nitride. The samples did not show dimensional or weight change, nor could corrosion attack be detected metallographically. The lithiumsaturated salt system did not show any behavior similar to that of liquid lithium corrosion. From testing in other gas compositions, it appears that the presence of oxygen in the system is necessary to produce severe corrosion. Order No.: JA905-044 © 1999 MRS

Elastic modulus measurement of multilayer metallic thin films K-H. Cho, Y. Kim

(Chonnam National University)

Two- and three-layer composite models were developed using a beam vibration theory, and the models were applied for measuring the Young's moduli of thin metallic films. The Cr, Ni, Co coated Si wafer composites (two-layer composite) and (Cr/Ti/Si)-composites (three-layer composite) were produced by radio-frequency (rf) magnetron sputtering and used to test the developed models. The Young's moduli of (Cr) films obtained by three-layer composite model agree well with those of (Cr) films obtained by two-layer composite model considering (Ti/Si) as the one layer and (Cr) as the other layer. This suggests that moduli of multilayer films may be obtained by using a two-layer composite model repeatedly. Order No.: JA905-045

© 1999 MRS

Iron oxide films of a spinel structure from thermal decomposition of metal ion citrate complex

N. Uekawa, K. Kaneko

(Chiba University)

The iron oxide films were prepared by the polymer precursor method with alkaline metal (Li, Na, K) ion doping. Alkaline metal ions were used to regulate the thermal decomposition process of the cation-citrate complex, that is, the precursor of the film. The spinel iron oxide films were obtained by firing the precursor with the alkaline ion doping [Na/Fe (atomic ratio) ≥ 0.2 and K/Fe $(\text{atomic ratio}) \ge 0.2$ at 773 K for 5 min in air. The formation mechanism of the spinel iron oxide films were investigated by differential thermal analysis (DTA) and x-ray photoelectron spectroscopy (XPS) measurements. The formation of the carbon-iron oxide complex was observed, and this reduction atmosphere induced the formation of the spinel iron oxide films. This method gave the spinel iron oxide films by which nanostructures are controlled. © 1999 MRS Order No.: JA905-046

Microcharacterization of liquid delivery metalorganic chemical vapor deposition processed thin film materials exhibiting giant magnetoresistance

M.L. Weaver,¹ L.P.M. Brandao,¹ H. Garmestani,¹ E.S. Gillman,² K.H. Dahmen,² A. Morrone³

(¹FAMU-FSU College of Engineering, ²Florida State University, ³University of Florida)

Thin films of La_{0.6}Ca_{0.4}MnO₃ (LCMO) have been produced on (001) oriented LaAlO3 (LAO) and yttrium stabilized zirconia (YSZ) substrates by liquid delivery metalorganic chemical vapor deposition (LD-MOCVD). X-ray diffraction (XRD) analyses showed that the films were epitaxially grown on LAO substrates and were monocrystalline at a thickness of less than 500 Å. At a thickness of greater than 500 Å, the films became polycrystalline but maintained their high texture (preferred crystalline orientation). Films grown on YSZ were always polycrystalline but were also highly oriented. Regardless of the substrate, the 1500 Å thick polycrystalline films exhibited substantially significant magnetoresistance ratios even above room temperature. © 1999 MRS Order No.: JA905-047

Microstructural evolution of dense and porous pyroelectric Pb_{1-x}Ca_xTiO₃ thin films

A. Seifert, L. Sagalowicz, P. Muralt, N. Setter (Ecole Polytechnique Fédérale de Lausanne)

 $Pb_{1-x}Ca_xTiO_3$ thin films with x = 0 - 0.3 for pyroelectric applications were deposited on platinized silicon wafers by chemical solution processing. Casubstitution for Pb in PbTiO₃ results in a reduced c/a ratio of the unit cell, which, in turn, leads to better pyroelectric properties. Control of nucleation and growth during rapid thermal annealing to 650 °C allowed the formation of either highly porous or dense (111) oriented films. The inclusion of pores creates a matrix-void composite with the low permittivity desired for pyroelectric applications, resulting in a high figure of merit. The growth mechanisms for the microstructural evolution of both dense and porous films were analyzed by x-ray diffraction transmission electron microscopy (TEM), scanning electron microscopy (SEM), and Rutherford backscattering spectroscopy and allowed establishment of microstructure/property relationships. © 1999 MRS Order No.: JA905-048

Micropyretic synthesis and leaching of MoSi₂ powders through an aluminothermic reaction

M. Fu,¹ S. Penumella,¹ J.A. Sekhar^{1,2}

(¹Micropyretics Heaters International, Inc., ²University of Cincinnati)

An aluminothermic reaction starting with inexpensive MoO₃, SiO₂, and Al powders was utilized to prepare molybdenum disilicide (MoSi2) powders by the micropyretic/combustion synthesis process and leaching. The combustionsynthesized product was porous, which could readily be crushed into powders. X-ray diffraction (XRD) analysis revealed that the product of such a reaction consisted of α -Al₂O₃, MoSi₂, and a small amount of Mo(Si, Al)₂ and Mo₅Si₃. The reason for the formation of $Mo(Si, Al)_2$ phase is discussed. $MoSi_2$ pow-ders were obtained by leaching out the Al_2O_3 from the synthesized powder mixtures in boiling phosphoric acid solution. The synthesized $MoSi_2$ powders, including a small amount of Mo(Si, Al)2 and Mo5Si3, were very fine with an average particle size of about 1 µm. Order No.: JA905-049

© 1999 MRS

Bombarding energy dependence of bonding structure in amorphous carbon interlayer and its effect on diamond nucleation

U.C. Oh,^{1,2} D.G. Cheng,¹ F.X. Lu,¹ J.H. Je²

(¹University of Science and Technology Beijing, ²Pohang University of Science & Technology)

The bombarding energy dependence of bonding structure in amorphous carbon interlayer and its effect on diamond nucleation density (N_d) were studied. Amorphous carbon (a-C) interlayer was deposited by magnetron sputtering. Interestingly, the intensity ratio (I_D/I_G) of the D band (~1400 cm⁻¹) to the G band (~1570 cm⁻¹) in the Raman spectra and the optical bandgap of the a-C film were found to be inversely proportional to the sputtering power, that is, to bombarding energy. When diamond was subsequently deposited at 800 °C by

microwave plasma chemical vapor deposition (CVD), diamond could be grown only on the interlayers with higher I_D/I_G [≥ 2.20], and N_d was increased up to 2×10^{6} /cm² with the increase of $I_{\rm D}/I_{\rm G}$ ratio, that is, with the decrease of the bombarding energy. We experimentally confirmed that the amount of the sp^3 bonded carbon clusters within the interlayer was dependent on the bombarding energy of the particles, determining the diamond nucleation density. We suggest that the transformation of the amorphous carbon into graphitic carbon should be effectively prevented for the diamond nucleation on the a-C interlayer. © 1999 MRS Order No.: JA905-050

The effect of growth condition on the structure of 2H-AlN films deposited on Si(111) by plasma-assisted molecular-beam epitaxy U. Kaiser,¹ P.D. Brown,² I. Khodos,³ C.J. Humphreys,² H.P.D. Schenk,¹ W. Richter¹

(¹Friedrich-Schiller-Universität Jena, ²University of Cambridge,

³Institute of Microelectronics Technology and High Purity Materials RAS) The effect of substrate cleaning, nitridation time, and substrate temperature in the range 800-1000 °C on the microstructure of AlN/Si(111) films grown by simultaneous plasma-assisted molecular-beam epitaxy have been investigated. It has been demonstrated using a combination of conventional and high-resolution transmission electron microscopy that the interface structure, the film defect structure, and the film surface roughness are strongly related. The formation of single-crystal 2H-AIN films with atomically flat surfaces occurs at 800 °C for conditions of 2.5 nm/min growth rate on very pure, atomically flat Si substrates. Order No.: JA905-051 © 1999 MRS

Low-temperature chemical vapor deposition of tantalum nitride from tantalum pentabromide for integrated circuitry copper metallization applications

X. Chen,¹ G.G. Peterson,¹ C. Goldberg,¹ G. Neusca,¹ H.L. Frisch,¹ A.E. Kaloyeros,¹ B. Arkles,² J. Sullivan³

(¹The University at Albany—SUNY, ²Gelest Inc., ³MKS Instruments Inc.) A low-temperature (<450 °C) thermal chemical vapor deposition (CVD) process was developed for the growth of TaN, from the reaction of tantalum pentabromide, ammonia, and hydrogen. Studies of process reaction kinetics yielded two sequential rate-controlling steps, with an activation energy of 0.45 eV for the kinetically limited reaction regime. Additionally, a systematic design of experiments approach examined the effects of key process parameters, namely, substrate temperature, source temperature, and hydrogen and ammonia flows, on film properties. A wide CVD process window was established for nitrogen-rich amorphous TaN_x with contamination below 1 at.%. Film conformality was higher than 95%in nominally $0.30 \,\mu\text{m}$, 4.5:1 aspect ratio, trench structures. Order No.: JA905-052

© 1999 MRS

The effects of capping barrier layers on the compositional and structural variations of integrated Pb(Zr,Ti)O₃ ferroelectric capacitor having the dimension $3 \times 3 \,\mu m^2$

C.S. Hwang,¹ J.C. Shin,¹ J.B. Lee,¹ J. Park,¹ Y.J. Cho,¹ H.J. Kim,¹ S.Y. Lee,² S.O. Park²

(¹Seoul National University, ²Samsung Electronics Co.)

Structure and composition of the ferroelectric Pb(Zr,Ti)O3 (PZT) layers in a capacitor of the ferroelectric random-access memory (FeRAM) device having a density of 64 k were investigated by transmission electron microscopy (TEM) together with the energy-dispersive spectroscopy (EDS) technique. The 250 nm thick PZT layer derived by sol-gel route showed a 2-3% Pb-deficient, 3-4% Ti-deficient, and 5-7% Zr-excess composition at the top electrode interface compared to the bulk composition when they were as-fabricated. The local compositional nonuniformity became more critical as the integration process proceeded, which seriously degraded the ferroelectric hysteresis and the device yield. The major cause of the compositional variation was the outward diffusion of Pb through the capping barrier TiO2 layer during annealing at 650 °C. AIN capping barrier layer was also not effective in suppressing the diffusion of Pb. However the Al2O3/TiO2 double capping layer was very effective in suppressing the outward diffusion of Pb and excellent ferroelectric characteristic was expected. Order No.: JA905-053

© 1999 MRS

Formation of C54-TiSi2 in titanium on nitrogen-implanted (001)Si with a thin interposing Mo layer

S.L. Cheng,¹ J.J. Jou,¹ L.J. Chen,¹ B.Y. Tsui²

(¹National Tsing Hua University, ²Industrial Technology and Research Institute) Formation of TiSi2 in titanium on nitrogen-implanted (001)Si with a thin interposing Mo layer has been investigated. The presence of Mo thin interposing

MRS BULLETIN/MARCH 1999

layer was found to decrease the formation temperature of C54-TiSi2 by about 100 °C. A ternary (Ti,Mo)Si2 phase was found to distribute in the silicide layer. The ternary compound is conjectured to provide more heterogeneous nucleation sites to enhance the formation of C54-TiSi2. On the other hand, the effect of grain boundary for decreasing transformation temperature was found to be less crucial. For Ti/Mo bilayer on 30 keV BF2+ or As+ + 20 keV, 1 × 1015/cm2 N2+ implanted samples, a continuous C54-TiSi2 layer was found to form in all samples annealed at 650-950 °C. The presence of nitrogen atoms in TiSi2 is thought to lower the silicide/silicon interface energy and/or the silicide surface energy to maintain the integrity of the C54-TiSi2 layer at high temperatures. Order No.: JA905-054 © 1999 MRS

Niobium and zirconium tellurides thin films prepared by sputtering D. Pailharey,¹ Y. Mathey,¹ M. Kassem^{1,2}

(¹Université de la Méditerranée, ²Atomic Energy Commission of Syria) A versatile procedure of sputter deposition, well-adapted for getting a large range of Te/M ratios (with M = Zr or Nb), has led to the synthesis of several highly anisotropic zirconium and niobium polytellurides in this film form. Upon turning the two key parameters of the process, i.e., the Te percentage in the target and the substrate temperature during the deposition, preparation of systems ranging from ZrTe_{0.72} to ZrTe_{6.7}, on the one hand, and from NbTe_{1.28} to NbTe_{7.84}, on the other, has been achieved. Besides their amorphous or crystalline (with or without preferential orientations) behavior and their relationship to known structural types, the most striking feature of these films is their large departure from the stoichiometry of the bulk MTe, reference compounds. This peculiarity, together with the possible changes of composition under annealing, are described and interpreted in terms of variable amounts of Te and M atoms trapped or intercalated within the parent structures. Order No.: JA905-055 © 1999 MRS

Structure and optical properties of diamondlike carbon synthesized by plasma immersion ion processing X-M. He, K.C. Walter, D.Q. Li, M. Nastasi

(Los Alamos National Laboratory)

Hard and transparent diamondlike carbon (DLC) films have been prepared on room-temperature substrates by using a C2H2-Ar plasma immersion ion processing (PIIP) method. The optical properties of the DLC films with different thickness deposited on PMMA (polymethyl methacrylate), silicon wafers, and glass plates were systematically examined. It was found that careful control of substrate bias voltage was needed for favorable growth of DLC films with low atomic hydrogen content, high hardness and wear resistance, and excellent optical properties. The resultant DLC films exhibited a low friction coefficient, high optical gap energy, and very high optical transmittance both in infrared and visible light ranges. The study confirmed that C2H2-Ar PIIP with low negative bias voltages and suitable C2H2/Ar gas ratios can produce optically transparent and hard DLC films on optical materials. Order No.: JA905-056

© 1999 MRS

Formation mechanism of spherical oxide particles containing dye S. Wu, C. Zhu

(Chinese Academy of Sciences)

2-[3-(1,3-dihydro-1, 3, 3-trimethyl-2H-indol-2-ylidine)-1-propenyl]-1,3,3trimethyl-3H-indolium idoide (HICI) dye-doped SiO₂ particles were synthesized by sol-gel method. Dimension, diameter, distribution, and homogeneity of the particles are closely related to the positively charged dye concentration, corresponding to the zeta potential of the particles. When the dye concentration reaches about 7.8×10^{-4} mol/mol SiO₂, corresponding to the isoelectric point of the particles, the maximum particle size and the most homogeneity can be reached. Order No.: JA905-057 © 1999 MRS

Preparation and enhanced photocatalytic oxidation activity of surface-modified CdS nanoparticles with high photostability M.Y. Han, W. Huang, C.H. Quek, L.M. Gan, C.H. Chew, G.Q. Xu, S.C. Ng (National University of Singapore)

Highly photostable CdS nanoparticles modified with alkyl group were prepared by an improved microemulsion technique using hexanethiol as cosurfactant. The surface-modified CdS nanoparticles catalyzed the photo-oxidation of 4-chlorophenol via continuously bubbling oxygen under uv light. The photocatalytic oxidation activity of the CdS nanoparticles was enhanced due to the formation of their compact CdS cores with strong chemical surface modification by heat treatment.

Order No.: JA905-058

The phase separation mechanism of CaO-B2O3-P2O5 in an electric field

W. Liu, X.M. Gu, K.M. Liang, H. Chen, Y.K. Zheng, S.R. Gu (Tsinghua University)

The effects of an electric field on phase separation in CBP (CaOB₂O₃P₂O₅) have been studied. It was discovered that an electric field can inhibit the process of phase separation in CBP glasses. If the electric field strength is increased, the inhibiting effect will increase, too. The mechanism of phase separation in an electric field has been discussed in light of the ir spectrum of CBP glasses. Order No.: JA905-059 © 1999 MRS

Structure-property behavior during aging of sol-gel derived silica modified with Si-H and Si-CH₃ groups

V.M. Sglavo,1 S. Diré,1 M. Ferrari2

(¹Università di Trento, ²Centro Fisca Stati Aggregati)

Unsupported films and thin rods were prepared by the sol-gel method from solutions of triethoxysilane and methyldiethoxysilane. Measurements of elastic modulus, density, glass transition temperature, and refractive index were performed at different aging times. Results showed a large increase of the elastic modulus with aging time which was related to the progressive condensation taking place in the xerogel network, as shown by solid state nuclear magnetic resonance (NMR). The stiffness increase was shown to correspond to higher glass transition temperature and larger density and refractive index. Different increasing rates of the physical and mechanical characteristics were observed for films and rods during aging. This behavior was related to the different loss rate of the pore liquid, which affects the network evolution in the wet gel. © 1999 MRS Order No.: JA905-060

Bulk amorphous Pd-Ni-Fe-P alloys: Preparation and characterization

T.D. Shen, Y. He, R.B. Schwarz

(Los Alamos National Laboratory)

Bulk amorphous alloys of $Pd_xNi_yFe_{80-x-y}P_{20}(25 \le x \le 60, 20 \le y \le 55,$ $x + y \ge 60$) were prepared by a flux-melting and water-quenching method. Seven mm diameter glassy rods of $Pd_{40}Ni_{40-x}Fe_xP_{20}$ ($0 \le x \le 20$) were studied in greater detail. For these alloys, the difference between the crystallization and glass transition temperatures ranges from 102 K for x = 0 to 53 K for x =20. In this composition range, the reduced glass transition temperature, T_{rg} , ranges from 0.66 to 0.57. The change in density upon crystallization ranges from 0.24 \pm 0.04% for x = 0 to 1.33 \pm 0.24% for x = 10. The partial molar volume of Fe in amorphous $Pd_{40}Ni_{40-x}Fe_xP_{20}$ alloys is significantly larger than the molar volume of (metastable) fcc Fe. This, as well as a comparison with the molar volumes of crystalline compounds, suggests chemically selective Fe-Pd bonding in these glasses. Order No.: JA905-061

© 1999 MRS

Pyrolysis of self-assembled organic monolayers on oxide substrates H. Shin,¹ Y. Wang,¹ U. Sampathkumaran,¹ M.R. DeGuire,¹ A.H. Heuer,¹ C.M. Sukenik²

(¹Case Western Reserve University, ²Bar Ilan University)

The pyrolysis of siloxy-anchored, organic self-assembled monolayers (SAMs) on oxide substrates [titanium dioxide powder; hydrolyzed silicon dioxide on (100) silicon] was studied using x-ray photoelectron spectroscopy (XPS), thermogravimetric analysis (TGA), and mass spectroscopy (MS). Pyrolysis in air began on heating at 200 °C and was complete by 400 °C for both octadecyltrichlorosilane (OTS) and C_{16} -thioacetate (TA) SAMs, as observed in TGA of SAM-coated TiO2 powders, and in XPS studies of TA-SAM-coated TiO2 powders and Si wafers after various heat treatments. In low-oxygen environments, pyrolysis of SAMs began at higher temperatures; between 250 and 400 °C for heating in ultrahigh vacuum (10-8 torr) as observed in XPS studies of TA-SAMs on Si, and between 300 and 400 °C in nitrogen, as observed in TEM analysis of sulfonate SAMs under a TiO₂ thin film on Si substrates. Order No.: JA905-062 © 1999 MRS

Anodic dissolution of diamondlike carbon film-coated type 301 stainless steel

C. Srividya, I. Moskowitz, S.V. Babu

(Clarkson University)

The resistance of thin diamondlike carbon (DLC) films to anodic breakdown in aqueous electrolytes was investigated using voltammetry. The films were less than 0.5 μ m thick and were deposited on type 301 stainless steel substrates using plasma-assisted chemical vapor deposition (PACVD) from either methane, acety-

lene, or 1,3-butadiene precursors with argon or hydrogen as diluent. A 10 nm thick polysilicon (PS) film was plasma-deposited prior to DLC film deposition to improve adhesion. The electrolytes used for corrosion testing were mixtures of 0.1 M NaCl, 0.1 M Na₂SO₄, 0.1 M HCl, and 0.1 M Na₂SO₄ in deionized water. The measured anodic current was lowest for the films deposited from butadiene and highest for those deposited from methane. The anodic current also increased with an increase in the hydrogen content in the feed gas mixture. In addition, the DLC films deposited at higher gas flow rates offered more resistance to anodic dissolution than those deposited at lower gas flow rates. Anneal-ing improved the film performance. There appears to be an optimum DLC film thickness which provides the maximum resistance to anodic dissolution. In the best case, the DLC films reduced the anodic dissolution of bare stainless steel by about four orders of magnitude in the passive region. Atomic force microscopy studies of coated and uncoated stainless steel showed that the DLC films conformed to the steel substrate surface and had no effect on surface roughness, while DLC coated silicon substrates showed no evidence of pores. Order No.: JA905-063 © 1999 MRS

Influences of thermal annealing and humidity exposure on

surface structure of (100) single-crystal MgO substrate M.P. Delplancke-Ogletree, M. Ye, R. Winand, J.F. de Marneffe, R. Deltour (Université Libre de Bruxelles)

We studied the influence of thermal annealing on the surface structure of (100) single-crystal MgO substrates by atomic force microscopy (AFM). By annealing MgO substrates at various temperatures for 4 h in flowing oxygen, we show that the surface reconstruction could be explained by considering surface diffusion, surface evaporation, and condensation. At an annealing temperature of 1473 K, a stepped structure was formed with screw dislocations acting as step sources. The influence of humidity on the surface morphology of MgO substrates was also studied by exposing them to a constant humidity of 40 and 80% for different times. After an exposure time of 1.5 h in 80% humidity, the substrate surface was already covered by reaction products. For the 40% humidity, the corresponding time is 10 h. The major reaction product was identified as Mg(OH)2 by x-ray diffraction. © 1999 MRS Order No.: JA905-064

Irreversible hydrogenation of solid C₆₀ with and without catalytic metals

E.L. Brosha, J. Davey, F.H. Garzon, S. Gottesfeld

(Los Alamos National Laboratory)

The dehydrogenation of $C_{60} \cdot H_{18.7}$ was studied using thermogravimetric and powder x-ray diffraction analysis. $C_{60} \cdot H_{18.7}$ was found to be stable up to 430 °C in Ar at which point the release of hydrogen initiated the collapse of a fraction of fullerene molecules. X-ray diffraction analysis performed on C60 • H18.7 samples dehydrogenated at 454, 475, and 600 °C displayed an increasing volume fraction of amorphous material. The decomposition product is comprised of randomly oriented, single-layer graphite sheets. Evolved gas analysis using gas chromatograph (GC) mass spectroscopy confirmed the presence of both H2 and methane upon dehydrogenation. Attempts to improve reversibility or reduce hydrogenation/dehydrogenation temperatures by addition of Ru and Pt catalysts were unsuccessful. Order No.: JA905-065 © 1999 MRS

Study on the structure of PbS nanoparticles coated with dialkyldithiophosphate

S. Chen, W. Liu, L. Yu

(Chinese Academy of Sciences)

PbS nanoparticles modified with di-n-hexadecyldithiophosphate (DDP) were prepared by chemical surface modification method. The structure of the PbS nanoparticles coated with DDP was investigated by means of infrared spectroscopy (ir), x-ray photoelectron spectroscopy (XPS), x-ray diffraction (XRD), transmission electron microscopy (TEM), and ³¹P nuclear magnetic resonance spectroscopy (31P NMR). The thermal stability of DDP coating on the PbS nanoparticles was compared with that of pyridinium di-n-hexadecyldithiophosphate (PyDDP) using a thermogravimetric analyzer (TGA). It was found that coated PbS nanoparticles had an average diameter of about 5 nm. Surface modification with DDP prevented water adsorption and effectively improved the dispersive capacity and antioxidative stability of PbS nanoparticles. The thermal stability of DDP coating on the surface of nano-PbS particles was higher than that of modifier PyDDP because of the chemical interaction between PyDDP and PbS during the coating process. © 1999 MRS Order No.: JA905-066

Determination of elastic modulus of thin films and small specimens using beam bending methods

J. Menčík, E. Ouandt

(Institute of Materials Research)

Elastic modulus of small specimens and thin films can be determined in bending tests using cantilever or three-point arrangement. The paper presents the basic formulae for these measurements, analyzes the errors which can arise, and shows how they can be reduced. The use of the method is illustrated on glass, silicon, and glass coated with TbDyFe. Order No.: JA905-067 © 1999 MRS

Electrodeposition of lithium phthalocyanine thin films: Part I. Structure and morphology

M. Brinkmann,¹ S. Graff,¹ C. Chaumont,² J-J. André¹ (¹Institut Charles Sadron,

²Institut de Physique et de Chimie des Matériaux de Strasbourg)

A new thin film synthesis route based on the electrochemical oxidation of PcLi2 and deposition of lithium phthalocyanine (PcLi) onto indium tin oxide (ITO) substrate is demonstrated. The effects on the thin film morphology of various parameters such as the electrolysis time, the nature of the solvent, and the oxidation potential are investigated. The thin film growth is studied via x-ray diffraction, potential step experiments, and ex situ scanning electron microscopy. Various morphologies of the x-form thin films are observed for different electrolysis times and solvents. Thin films grown in acetonitrile of thickness above approximately 1 µm consist in unidirectionally oriented needle-shaped crystallites. Order No.: JA905-068 © 1999 MRS

Fracture toughness of diamondlike carbon coatings

M. Nastasi,¹ P. Kodali,¹ K.C. Walter,¹ J.D. Embury,¹ R. Raj,² Y. Nakamura³ (¹Los Alamos National Laboratory, ²University of Colorado, ³Kagoshima University)

The fracture behavior of diamondlike carbon (DLC) coatings on Si substrates has been examined using microindentation. The presence of DLC coatings reduces the radial crack length to less than one half the crack length

observed in uncoated Si at the same indenter load. A total work of fracture analysis of the radial cracks formed in the DLC-coating/Si-substrate system gives 10.1 MPa m^{1/2} as the average fracture toughness for DLC alone. A bond breaking calculation for DLC suggests that the elastic limit fracture toughness should be 1.5 MPa $(m)^{1/2}$. The higher value obtained from experiment and total work analysis suggests that plastic work and/or a torturous path crack evolution occurred during DLC fracture process. Order No.: JA905-069 © 1999 MRS

Microstructure modification of amorphous carbon films by ion-implantation techniques

B. Wei, K. Komvopoulos, I.G. Brown

(University of California-Berkeley)

Microstructure modification of amorphous carbon films containing about 30 at.% hydrogen (a-CH,) and nonhydrogenated amorphous carbon (a-C) films was accomplished with a vacuum arc metal plasma implanter and a cathodic arc plasma system, respectively. The films were implanted with Si, Ti, Hf, W, and Al of ion doses approximately equal to 1 and 3×10^{16} ions/cm² and mean ion kinetic energies in the range of 3-70 keV, depending on the implantation method. Simulation results demonstrated a profound effect of the size of implant species, ion dose, mean ion kinetic energy and implantation processes on the implant spatial distributions. Statistical roughness results showed a negligible effect of ion implantation on the film surface topography. Elastic recoil spectroscopy revealed a decrease in the hydrogen content of the a-CH, films due to the ion bombardment. A monotonic decrease in the Raman scattering intensities and a downward shift of the carbon peak position occurred with increasing ion dose for both types of films and implantation techniques. Nanoindentation experiments demonstrated an effect of ion implantation on the apparent film hardness, depending on the flux and kinetic energy of implanted species. Changes in the hardness characteristics of the implanted films are interpreted in terms of the chemical reactivity of implant elements and microstructure modifications caused by irradiation damage, dehydrogenation, and higher contents of tetrahedral (sp3) carbon hybridization due to carbide bond formation.

Order No.: JA905-070

© 1999 MRS

Please use the convenient postcard located in the back of the MRS Bulletin to order JMR reprints. When ordering single article reprints please note they are not available until the issue is published. See JMR Abstracts on the MRS Website at http://www.mrs.org/publications/jmr/jmra/.

GET CONNECTED

BENEFITS OF MEMBERSHIP

Two Annual MRS Meetings

As an MRS member, you'll automatically receive the Call for Papers and Program for upcoming meetings, as well as discounted MRS Meeting registration rates

MRS Bulletin

The MRS Bulletin is your free monthly publication with timely news and features on the research and development of advanced materials.

Journal of Materials Research

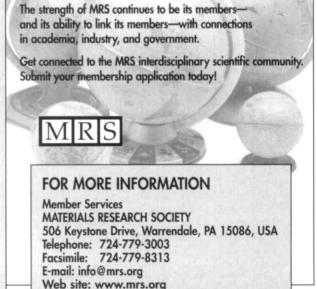
Yours for a very low member rate, Journal of Materials Research is an international archival journal encompassing physical, chemical, and engineering research on advanced materials and processing techniques.

MRS Books & Videotapes

As an MRS member, you may purchase MRS books and videotapes at 15-30% below list price. You'll also enjoy reduced rates for journals and books from other scientific publishers.

Opportunities to Connect

- Career services for members include the Job Center at MRS Spring and Fall Meetings.
- The annual Membership Directory is your connection to over 12,400 MRS members worldwide
- Reduced membership renewal and meeting fees are available to unemployed or retired members, as well as recent graduates as yet unemployed.



980097